Global and Planetary Change 110 (2013) 386–396

Contents lists available at ScienceDirect

Global and Planetary Change

journal homepage: www.elsevier.com/locate/gloplacha

Discovery of Holocene millennial climate cycles in the Asian continental interior: Has the sun been governing the continental climate?

Vadim A. Kravchinsky [a,b,*], Cor G. Langereis [b], Shawn D. Walker [a], Konstantin G. Dlusskiy [c,1], Dustin White [c,2]

[a] Department of Physics, University of Alberta, Edmonton, Alberta T6G 2G7, Canada
[b] Department of Earth Sciences, Utrecht University, Budapestlaan 17, 3584 CD Utrecht, The Netherlands
[c] Department of Anthropology, University of Alberta, Edmonton, Alberta T6G 2H4, Canada

ARTICLE INFO

Article history:
Received 29 July 2012
Accepted 24 February 2013
Available online 24 March 2013

Keywords:
bond cycles
climate
environmental changes
Holocene
loess
magnetic susceptibility
petromagnetism
Siberia
soil
solar insolation

ABSTRACT

We conducted a high-resolution study of a unique Holocene sequence of wind-blown sediments and buried soils in Southern Siberia, far from marine environment influences. This was accomplished in order to assess the difference between North Atlantic marine and in-land climate variations. Relative wind strength was determined by grain size analyses of different stratigraphic units. Petromagnetic measurements were performed to provide a proxy for the relative extent of pedogenesis. An age model for the sections was built using the radiocarbon dating method. The windy periods are associated with the absence of soil formation and relatively low values of frequency dependence of magnetic susceptibility (FD), which appeared to be a valuable quantitative marker of pedogenic activity. These events correspond to colder intervals which registered reduced solar modulation and sun spot number. Events, where wind strength was lower, are characterized by soil formation with high FD values. Spectral analysis of our results demonstrates periodic changes of 1500, 1000 and 500 years of relatively warm and cold intervals during the Holocene of Siberia. We presume that the 1000 and 500 year climatic cycles are driven by increased solar insolation reaching the Earth surface and amplified by other still controversial mechanisms. The 1500 year cycle associated with the North Atlantic circulation appears only in the Late Holocene. Three time periods — 8400–9300 years BP, 3600–5100 years BP, and the last ~250 years BP — correspond to both the highest sun spot number and the most developed soil horizons in the studied sections.

1. Introduction

Although a number of high-resolution climatic studies of the ocean and various continental parts, especially North Atlantic regions, explain climatic variability in the Holocene, it is still unknown how Eurasian climatic changes in the continental interior fit these models. Of the Earth's continental sedimentary successions, the Holocene Siberian loess/soil sequence presented in this study is most remote from oceanic influence.

The climate of the North Atlantic is strongly controlled by the mixing of waters from different ocean basins. This mixing is triggered by a mechanism called thermohaline circulation (Rahmstorf, 2006). The movement of ocean water in thermohaline circulation depends on variations in temperature and salinity. Climate cyclicity through the Holocene has been observed only in or near marine settings and is strongly controlled by glacial input to the North Atlantic (Bond et al., 1997). Periodicities of ~2500, ~1500, and ~1000 years are generally observed in the North Atlantic (Bond et al., 1997; Bianchi and McCave, 1999; Schulz and Paul, 2002; Viau et al., 2006; Debret et al., 2009). Insolation with a 900-year component has been proposed to be a potential driving force for the ~1000-year cycles (Schulz and Paul, 2002). The glacial material influx influenced by solar variability has been proposed to be the cause of the 1500-year cycles recorded in the North Atlantic (Bond et al., 2001).

It is still questionable if such periodicities and well-documented North Atlantic events like the Little Ice Age or the Medieval Warm Period were manifest in the continental interior of the largest continent, Asia. As interior Asia is remote from oceanic influence, the effects of solar variability could be more pronounced compared to near-marine environments like Europe or North Atlantic regions (Kravchinsky et al., 2007, 2008). Logistic complexity in sample collection on available sedimentary sections may account for the dearth of high-resolution data from continental Asia.

2. Site description

A continuous Holocene soil/loess section was sampled in the Trans-Baikal region of Siberia (Fig. 1). The Burdukovo site is situated

* Corresponding author at: Department of Physics, University of Alberta, Edmonton, Alberta T6G 2G7, Canada. Tel.: +1 780 492 5591; fax: +1 780 492 0714.
E-mail address: vadim@ualberta.ca (V.A. Kravchinsky).
[1] Now at Solstice Canada Corp., Edmonton, Alberta T5M 0H1, Canada.
[2] Now at Archaeology, University of Southampton, Southampton SO17 1BJ, UK.

0921-8181/$ – see front matter © 2013 Elsevier B.V. All rights reserved.
http://dx.doi.org/10.1016/j.gloplacha.2013.02.011

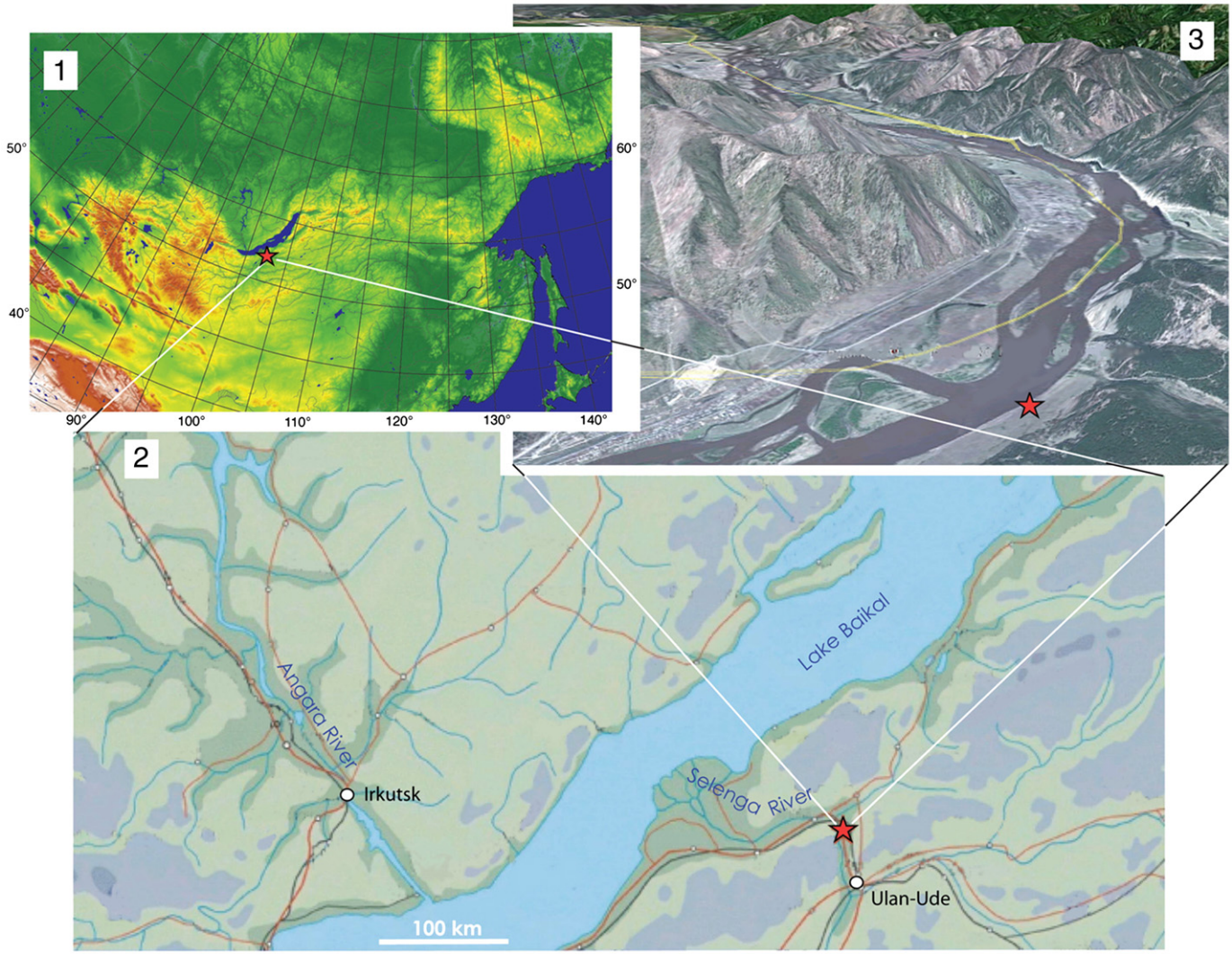

Fig. 1. Location of the Burdukovo study site. An insert shows the site at a large scale. Plotted using Google Earth.

at a terrace in the Selenga River valley, east of Lake Baikal (52.1°N and 107.5°E), just outside the village of Burdukovo. Four trenches were dug in the terrace to allow construction of a 5 m composite cross-section. The most prominent buried soils were traced along the terrace forming a series of small paleo-depressions and plateaus and were used as correlation levels between the trenches (Fig. 2). The soil descriptions are based on the Canadian System of Soil Classification (Soil Classification Working Group, 1998), with the WRB international classification equivalents provided in brackets (International Society of Soil Science, 1998) following White et al. (2013). The modern soil is a Eutric Brunisol (Eutric Cambisol). The buried soils are Cumulic Humic Regosols (darker horizons) and Cumulic Regosols (Mollic Fluvisols and Cumulic Arenosols).

Trench 1 was located near the base of a paleo-depression and was 4.05 m from the top of the terrace to the bottom of the trench (Fig. 2). Trenches 2 and 4 repeat each other and were both located in the transition zone of a paleo-depression. Trench 3 was at a plateau and exposed 3.45 m of sediment. Trench 4 was 4.40 m from the top of the terrace to the bottom of the trench and contained the contact between the Holocene deposits and earlier alluvial sand and gravel.

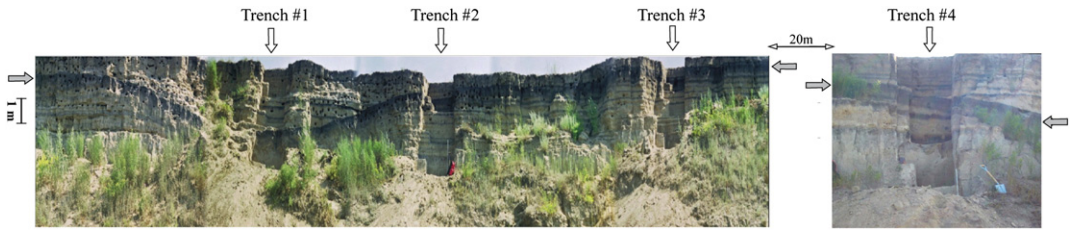

Fig. 2. The Burdukovo study site trenches. Trench 1 is at the base of the paleo-depression, Trenches 2 and 4 are in a transitional zone, Trench 3 is on a plateau. The gray horizontal arrows on either side of the figure are indicating the top of soil #13, the thickest buried soil. As the best developed buried soil, it was used as the datum for correlation of the units between the individual trenches.

Only well-developed buried soils shown in the composite cross-section of Fig. 3 contain A and B horizons. Other soils do not have enough maturity and are very thin. Discontinuity affiliated with the soil horizon 13 was observed in the micro paleo-depressions (Trenches 1, 2 and 4). The loess on the plateaus appears to be continuous but missing the top of the composite section.

Samples of $2 \times 2 \times 2$ cm^3 were taken continuously at 2.5 cm intervals. Section (trench) sampling overlapped by 1 m to verify the repeatability of measured properties for the same stratigraphic levels.

3. Methods

To identify variations in the concentration, grain size, and mineralogy of the magnetic material in the sections, petromagnetic parameters — low field mass specific magnetic susceptibility (MS) χ_{lf}, frequency dependence (FD) of magnetic susceptibility, anhysteric remanent magnetization (ARM), saturation isothermal remanent magnetization (SIRM), and back field isothermal remanent magnetization (bIRM) — and the ratios derived from them (normalized to the steady field anhysteric remanent magnetization χ_{ARM}, and S-ratio were measured in the paleomagnetic laboratory of the Physics Department at the University of Alberta (see Supplementary Materials for further details).

A number of special precautions have been taken during FD measurements to suppress the usually quite high noise level of the Bartington instrument. First of all every sample has been measured at least three times in different positions and the MS averages have been used in all further figures. All three MS measurements were fairly consistent and with no unusually high errors. The FD value was calculated from the average low- and high frequency MS values for every sample. We measured the samples with extra care during the evenings when the electromagnetic noise was lowest in the lab. The instrumental drift was also monitored and eliminated by taking 'air' readings before and after each sample measurement.

Sedimentary grain size was measured on a Sedigraph 5100 available at the Earth and Atmospheric Sciences Department (University of Alberta) (see Supplementary Materials for more details on sedimentary grain size analysis).

Samples for radiocarbon (^{14}C) dating were collected as part of a previous study of the site (White, 2006; White et al., 2013). Analyses were carried out by ISOTRACE Laboratories with results derived either from bulk soil material or charcoal fragments, the latter dated by accelerator mass spectrometry (AMS). Sample proveniences are associated generally with Trench 4. The uncorrected ^{14}C dates were calibrated using OxCal software version 3.10 (Ramsey, 2001) following a technique described in Ramsey (2001) and Reimer et al. (2004). The calibrated ages are listed in Table 1. The composite depth was converted to the age by linear interpolation between the radiocarbon dates. Preliminary optically stimulated luminescence (OSL) dating for the

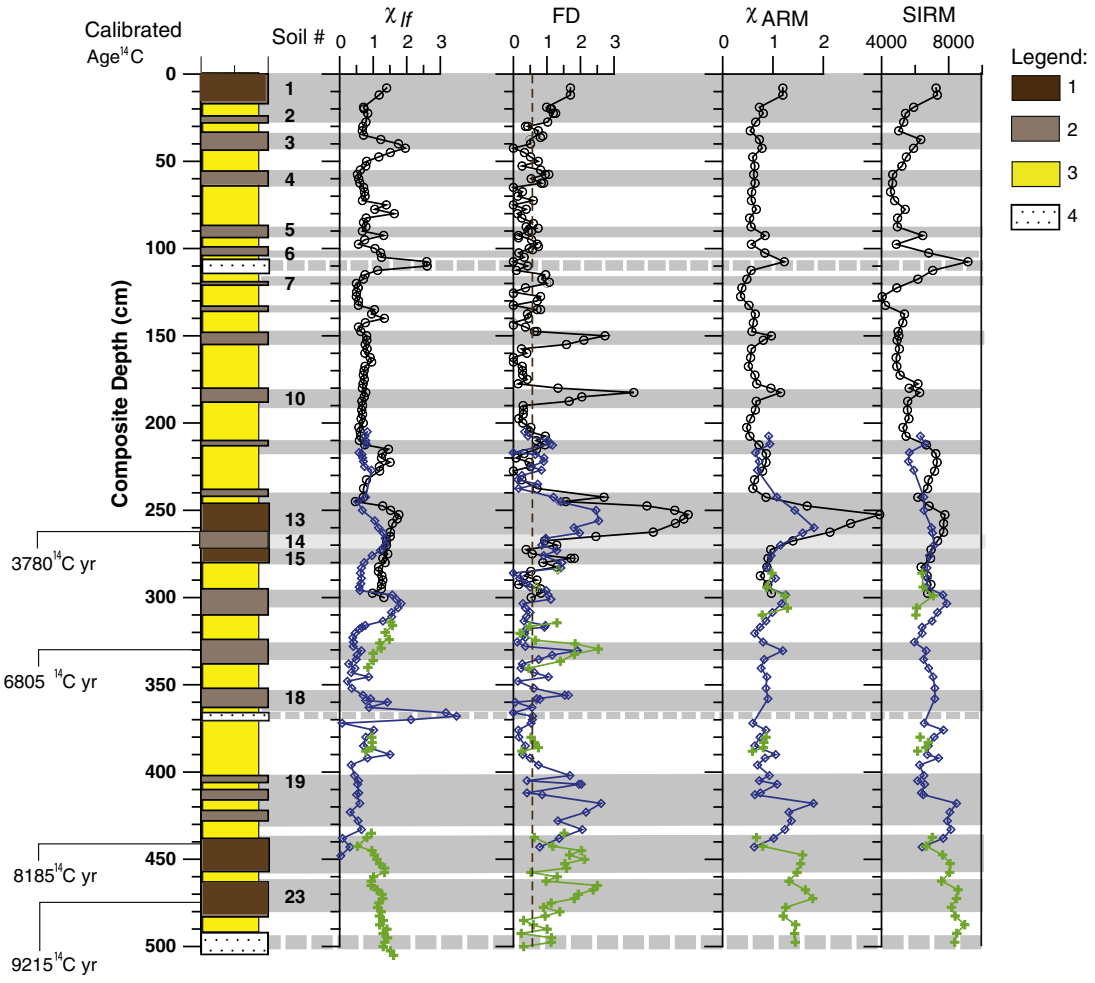

Fig. 3. Section description and magnetic concentration parameters for Burdukovo site. χ_{lf} — low frequency magnetic susceptibility (10^{-6} m^3 kg^{-1}); FD — frequency dependence parameter (%); χ_{ARM} — anhysteric remanent magnetization (10^{-6} m^3 kg^{-1}); and SIRM — saturation isothermal remanent magnetization (10^{-6} Am^2 kg^{-1}). See supplementary material section Methods for detailed explanation of petromagnetic parameters. Black (blue, green) symbols correspond to Trench 1 (3, 4). Legend: 1(2) — organic rich dark (poor developed light color) soil, 3 — loess horizons, and 4 — sandy layers. Dotted line in FD parameter denotes the mean FD (0.61%). Horizontal solid (dashed) gray lines denote soil (sandy) horizons.

Table 1
Calibrated ^{14}C ages in years BP.

Composite depth (cm)	Uncalibrated age (years)	Calibrated age (years)
265	3500 ± 70	3780 ± 90
330	5970 ± 60	6805 ± 145
442	7370 ± 70	8185 ± 165
475	8230 ± 120	9215 ± 185

loess samples from the composite depth level of 1.7, 3.4 and 3.9 m endorses the here reported ^{14}C ages. The result of the OSL dating is a subject of a separate publication under the auspices of the Chinese colleagues (personal communication). Non-linear time scales were also tested assuming soil to have higher or lower sedimentation rates than loess and taking in account the possibility of a discontinuity at horizon 13. The linear model was still the most robust representation of the mean sedimentation rates on the secular — millennium scale of this study. Only for the dark and organically rich soil horizons did we assume a slightly slower (~20%) sedimentation rate. The pedogenic magnetic mineral formation does not usually occur exactly on the top of the new-forming soil; observed FD peaks therefore may appear older than they actually are. The top layer could then be removed and re-deposited during cooler and windier periods exposing the magnetic minerals to the surface. It is unfeasible to estimate the exact influence of such process on our age model, however the duration of the soil horizon formation is in the order of 100 years in our study and the FD signal is still sufficient.

4. Results

All measured parameters are plotted against the composite cross-section in Figs. 3 and 4. The section was constructed by visual correlation of the soil horizons which could be easily traced from

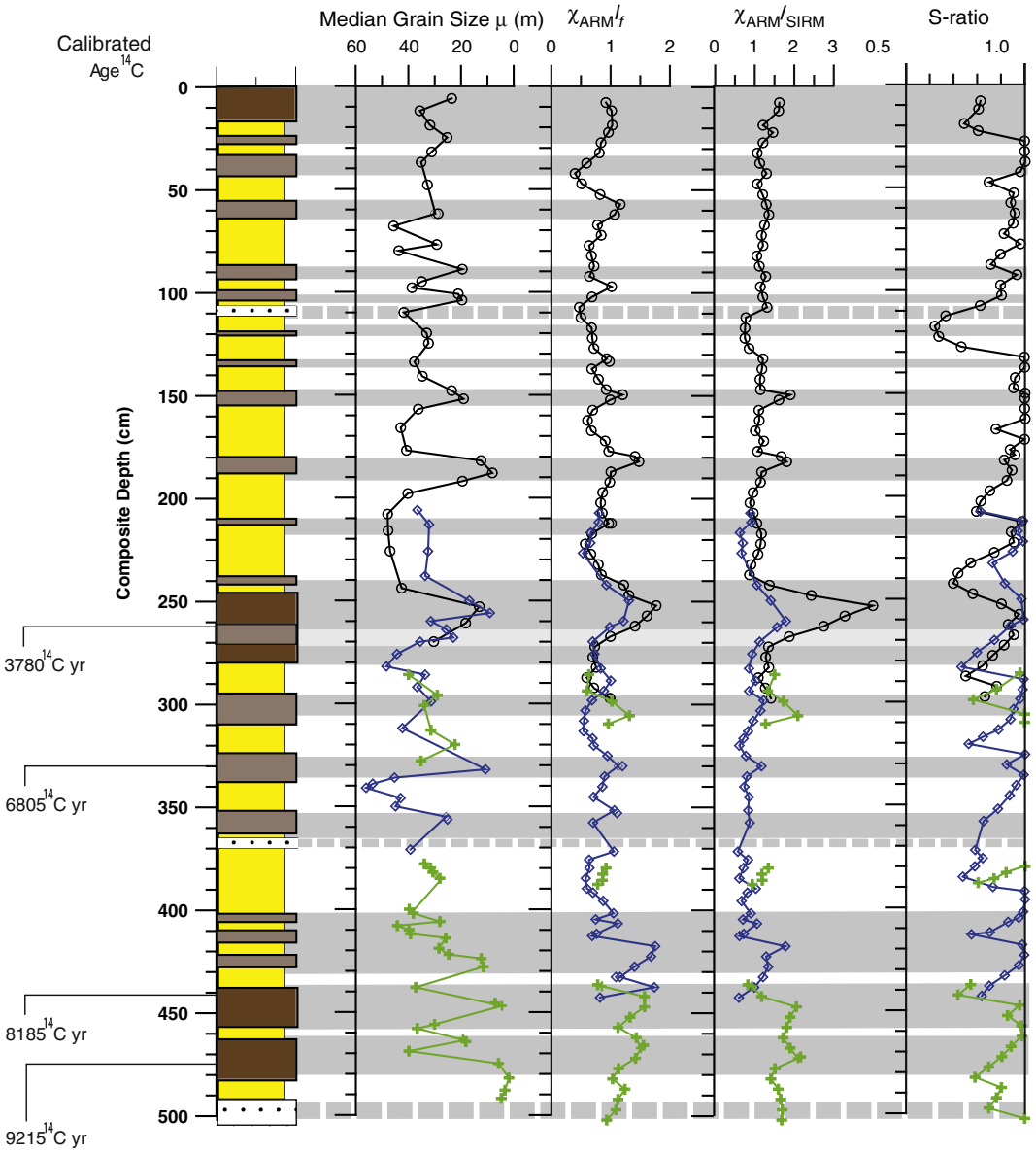

Fig. 4. Section description and analytic data for Burdukovo site. Grain size — median sedimentary grain size (μm); χ_{ARM}/χ_{lf} (unitless) and χ_{ARM}/SIRM (10^{-4} mA^{-1}) — magnetic concentration parameters; and S-ratio (unitless) — magnetic mineralogy parameters. See supplementary material section Methods for detailed explanation of petromagnetic parameters. Black (blue, green) symbols correspond to Trench 1 (3, 4). Same legend as in Fig. 3.

trench to trench in the field (see highlight of the soil horizons of Trench 1 in Supplementary Materials, Fig. SM-1, and an ink sketch highlighting the major soil horizons in the different trenches and their continuation from trench to trench in Fig. SM-2). Fig. 3 demonstrates that magnetic susceptibility often but not always correlates with soil horizons. Possible reasons for the lack of correlation between soil intervals and MS values for Siberian loess sections are discussed in Kravchinsky et al. (2008) and Bábek et al. (2011). MS reveals a close relationship to the redox capacity during pedogenesis and the type of soil. One of the most common complexities obscuring correspondence between paleosols and magnetic susceptibility is gleization which was observed in the studied sections along with ferruginous mottles. Some of the soils in the upper part of the section were formed during short time periods and are thin and weak to develop a strong magnetic susceptibility signal.

The frequency dependence (FD) parameter (Fig. 3) appears to correspond to the most prominent soil intervals. FD has become the leading parameter for analyzing climatic change in Siberian sequences (Kravchinsky et al., 2008) because it is higher in soil horizons than in loess. The enhanced FD parameter in soils is associated with ferromagnetic minerals, mostly superparamagnetic magnetite produced during pedogenesis. For the interval between 0.5 and 1.2 m, however, the soil horizons were thin and weakly developed and their correspondent FD peaks barely exceed the mean value of 0.61%. All other FD peaks are characterized by values of more than 1%. Very well developed and relatively thick soil horizons have FD values ranging from 2 to 6%.

Magnetic concentration parameters χ_{ARM} and SIRM (Fig. 3) confirm the presence of FD peaks that correspond to soil horizons at 150, 185, and 330 cm where χ_{lf} does not show any variations. Especially χ_{ARM} shows a higher concentration at the corresponding depths.

The sedimentary grain size in Fig. 4 demonstrates the general correspondence of the smaller median grain size values to the soil horizons. Larger median grain sizes correspond to the loess layers. The stronger wind during the relatively cooler periods of the loess accumulation displaced larger sedimentary particles when the vegetation was poorly developed and pedogenesis processes were weak. In such colder intervals it was easier for the wind to lift and transport sedimentary grains further and they accumulated in local topography depressions like the Burdukovo site. This scenario agrees with the wind vigor model suggested by Evans and Heller (2001) for Siberian loess deposits.

Parameters that characterize the magnetic grain size (χ_{ARM}/χ_{lf} and χ_{ARM}/SIRM) demonstrate smaller sizes for the well-developed and thicker soil horizons at 150 cm and below confirming the sedimentary grain size peaks. The thin soil layers above 150 cm appear to be too weak in terms of magnetic mineral development to show well-defined peaks, although the sedimentary grain sizes in these soils are small for this depth interval.

A higher S-ratio parameter corresponds to a higher amount of low coercivity magnetic minerals (i.e., magnetite and maghemite) in a sample. The S-ratio curve indicates that on the soil/loess interval time scales the ratio of low coercivity to high coercivity magnetic minerals is mainly controlled by variations in the production of pedogenic magnetite/maghemite superimposed on a hematite/goethite background. Newly produced magnetite in the soils concurs with a higher rate of weathering-produced hematite during soil formation time intervals.

5. Discussion

The results of petromagnetic studies of the Burdukovo Holocene section reveal two distinct sedimentary and magnetic mineral assemblages (Table 2). The magnetic concentration parameters correspond consistently to well-developed soils below 150 cm depth. Such soil intervals are characterized by higher magnetic concentrations and FD parameters that signify conventional production of magnetic minerals during soil formation. During relatively cooler intervals, eolian input prevails in the concentration of magnetic minerals.

Magnetic and sedimentary grain sizes vary in a very similar manner. Smaller grain sizes correspond to soil intervals and larger grain sizes correspond to loess intervals. This might indicate stronger winds during relatively cool and dry periods. Winds lift larger sedimentary grains from the ground when the vegetation and soil development is weak and unable to prevent erosion. Sedimentary grain size appears to be a more sensitive indicator of wind strength for the uppermost interval (above 150 cm) refining the magnetic parameter indication of more recent and weakly developed soils.

The magnetic mineral composition variations do not correspond to the soil intervals entirely. The correspondence is probably diluted by secondary alterations where magnetite is transformed to hematite. Evidence of this process was observed in the reddish or brown tone of the soils, and is known to occur in Chinese paleosoils (Bloemendal and Liu, 2005).

In order to perform spectral analysis and evaluate Holocene climatic periodicities, we used the FD factor because it identifies the most developed soil intervals better than other parameters. The three studied sections were combined by putting their FD data on a common age scale by linear interpolation between the correlation points and averaging the two values whenever their ages were identical. The resulting curve was smoothed by the least squares method to reduce discrepancies in the values between different sections.

We compare our resulting lithology, FD and sedimentary grain size records with reconstructed sunspot number (Solanki et al., 2004), the amount of solar modulation (Vonmoos et al., 2006), and the Lake Baikal $\delta^{18}O$ values from diatom silica (Mackay et al., 2011) (Fig. 5). Sunspot numbers for the Holocene have been reconstructed using dendrochronology and radiocarbon dating (Solanki et al., 2004). All soil intervals visually correspond to the higher sunspot number and amount of solar modulation very well. The level of solar activity during the past 70 years is extraordinarily high and is comparable to a period of similar high magnitude that occurred ~2500, 3600–4000, ~5100 and ~9000 years ago (Solanki et al., 2004). At Burdukovo, the richest organic, thicker, and darker soils correspond to three intervals: near the present day, 3600–5100 years ago (three-layer soil), and 8400–9300 years ago (double soil).

The double soil coincides, for example, with paleohydrological changes found in west-central Europe (Magny et al., 2011) where higher lake-level conditions existed until 9000 years BP, followed by a maximal lowering at 8500–9000 years ago. The triple weakly developed soil at 7500–8000 years BP (Fig. 5) correlates well with the Laurentide Ice Sheet retreating identified using ^{10}Be (Carlson et al., 2007). The whole interval 7500–9300 years BP corresponds generally to the warmer temperature interval registered in the Greenland ice record that reveals a pronounced Holocene climatic optimum coinciding with maximum thinning near the Greenland ice sheet

Table 2
Generalized characteristics of the two sedimentary assemblages for the studied Holocene section.

Parameter	Interglacial assemblage	Glacial assemblage
Lithology	Soil	Loess
Magnetic concentration (χ_{lf}, χ_{ARM}, SIRM)	Higher	Lower
Magnetic concentration of superparamagnetic particles FD-factor	Higher	Lower
Magnetic grain size χ_{ARM}/χ_{lf} χ_{ARM}/SIRM	Higher proportion of smaller size magnetic grains	Lower proportion of smaller size magnetic grains
Sedimentary grain size	Higher proportion of smaller sedimentary grains	Lower proportion of smaller sedimentary grains

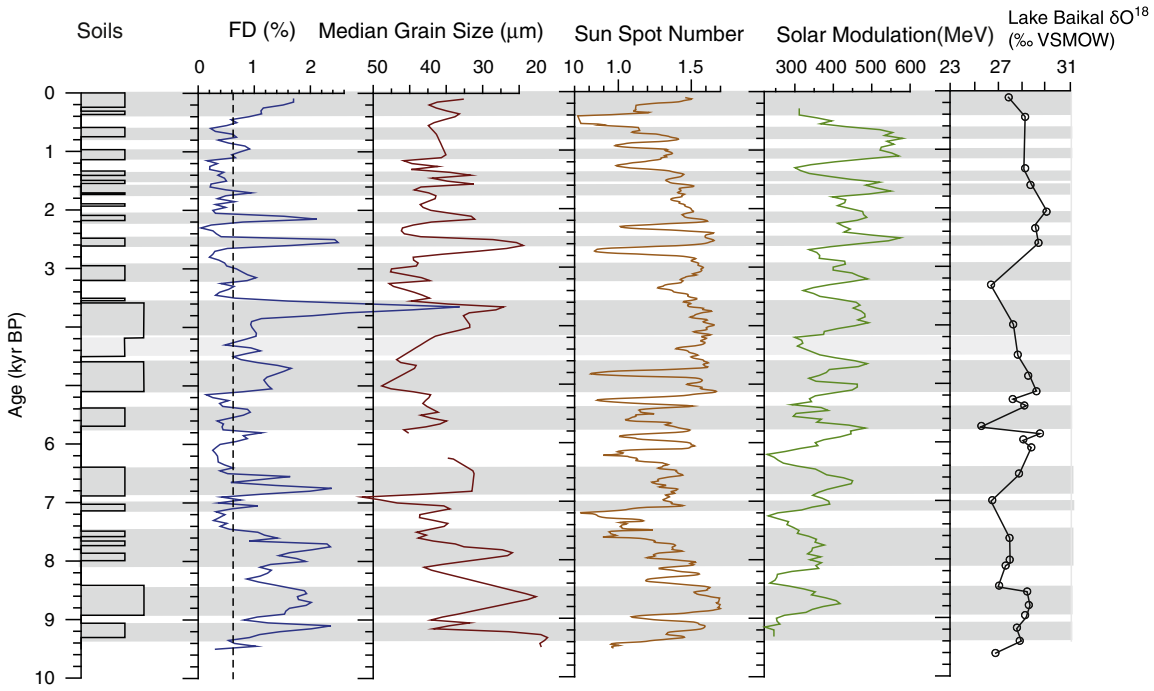

Fig. 5. Comparison between frequency dependence (FD) parameter, median grain size and buried soil horizons for Siberian Holocene loess/soil sequence (this study) and sun spot number defined from dendrochronologically dated radiocarbon concentrations (Solanki et al., 2004), amount of solar modulation in mega electron volts (Vonmoos et al., 2006) and Lake Baikal $\delta^{18}O$ profile linked to mass-balancing isotope measurements in per mil deviations from VSMOW (Vienna Standard Mean Ocean Water) (Mackay et al., 2011). Logarithm of the sun spot number is used to highlight the variations. Thickness of the soils was assessed visually in the field.

margins (Vinther et al., 2009). Tarasov et al. (2007) reported the warmest and wettest climate at ~7000–9000 years BP in the Lake Baikal region.

The other triple organic rich soil interval of ~3600–5100 years ago also corresponds both to the longest interval with high sun spot numbers in the Holocene (Solanki et al., 2004) in Fig. 5 and the Drift Ice Indices Stack and amount of ^{10}Be from the North Atlantic (Bond et al., 2001) in Fig. 6. Although the resolution of the $\delta^{18}O$ data from Holocene sediments of Lake Baikal is not very high (Mackay et al., 2011), there are no other detailed records in the study area to compare with. The major episodes are in good agreement with our records (Fig. 2). The Baikal record highlights the dominance of fluvial input between 5300 and 4000 years BP, which may indicate a relatively warm period with higher precipitation in the Lake Baikal region. The Siberian pollen record (Tarasov et al., 2007) provides additional evidence for associating the warmer and moister climate at 5600–4000 years BP with the mature soil formation in the study section (horizons 13–15).

Day et al. (2007) hypothesized that approximately one millennium after 7 kyr BP slowing of sea-level rise and gradual increase in temperatures, many coastal urban centers started to develop around the world. They correlated it with the development of stable coastal environments and ecosystems and an increase in marine productivity, which would provide a food source for hierarchical urban societies. The warmer global climate conditions also led to the expansion of agriculture and population growth in interior regions, forming some of the first large urban societies in many parts of the world (Staubwasser and Weiss, 2006), whereas the impact of climate drying and consequent decrease in rainfall following this period often reduced agricultural productivity in some regions (DeMenocal, 2001). The earliest human civilizations in Africa, the Middle East, and Asia were just beginning to rise 3500–5200 years BP which appears to coincide with the organic rich triple soil interval of 3600–5050 years BP indicating a globally registered warming period.

At present, some degree of skepticism about the climatic impact on human civilizations still exists in the literature for particular cases, and it has also been demonstrated that ancient society collapses might be strongly nonlinear in character, driven by complexities within a self-organizing structure of the society. It is not always obvious if the climate change was the typical trigger for the collapse (Coombes and Barber, 2005). Therefore obtaining and analyzing high-resolution palaeoenvironmental records may help illuminate this debate.

Beer et al. (2006) reconstructed a 9000-year record of solar modulation by removing the effect of the changing geomagnetic field on the production rate of ^{10}Be. They compared their solar modulation record with other paleoclimatic data and reported a causal link between solar variability and climate change in the Holocene, although the underlying physical processes that caused the relationship are not clear. The most promising candidate is changing in cloud formation because clouds have a very strong impact on the radiation balance and because only little energy is needed to change the cloud formation process. One of the ways to influence cloud formation might be through the cosmic ray flux that is strongly modulated by the varying solar activity (Friis-Chrisensen and Svensmark, 1997). More recently, Gallet et al. (2003) discussed possible periods of rapidly increasing geomagnetic field intensities from 5000 to 2000 years BP which they called 'archaeomagnetic jerks'. The visual correlation of these short peaks to cooling episodes in the North Atlantic (Bond et al., 1997, 2001) led Gallet et al. (2006) to suggest that the geomagnetic field may have had an impact on climate and therefore perhaps even on the history of ancient civilizations: major cultural crises would occur at the end of cooling cycles — causing arid conditions — which in turn would coincide with rapidly increasing geomagnetic field intensity, both in Mesopotamia and the Levant, and possibly during Mayan history as well (Gallet and Genevey, 2007). On the basis of this temporal coincidence, Courtillot et al. (2007) argued that there may have been a connection between Earth's magnetic field and climate. A proposed mechanism involves variations in the geometry of the geomagnetic field resulting in enhanced cosmic-ray induced nucleation of clouds. This speculation has led to heated debates on potential mechanisms causing climate change in the past (Bard and Delaygue, 2008; Courtillot et al., 2008).

The main features of the FD profile resemble the oceanic record as well (Stack of Drift Ice Indices), ^{10}Be records from Bond et al. (2001),

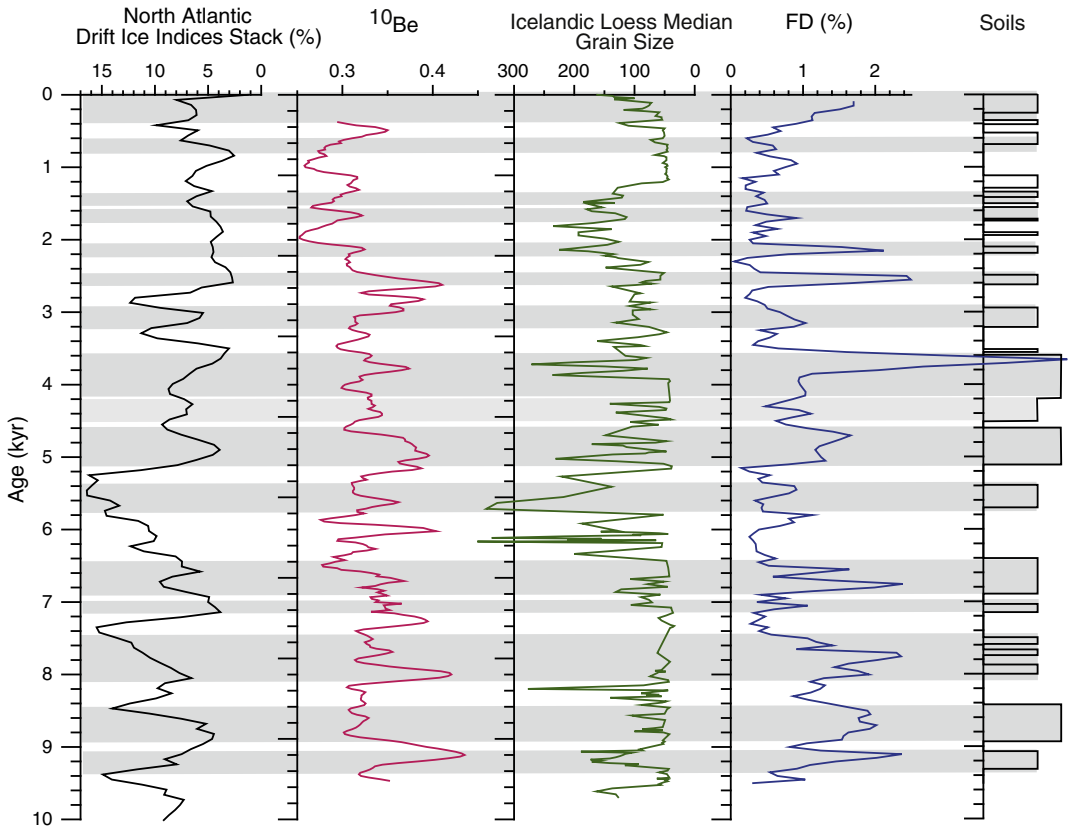

Fig. 6. Comparison between Drift Ice Indices Stack and amount of ^{10}Be from North Atlantic (Bond et al., 2001), median grain size from loess section of Iceland (Jackson et al., 2005), frequency dependence (FD) parameter and buried soil horizons for Siberian Holocene loess/soil sequence (this study).

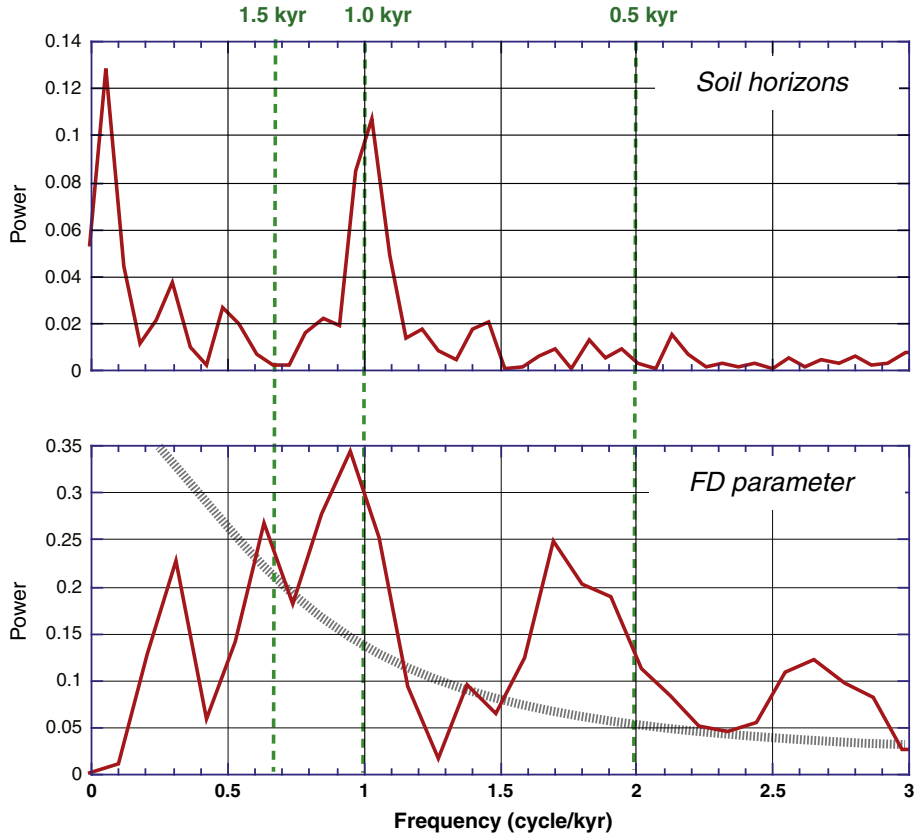

Fig. 7. Comparison between Walsh transform spectra for the lithological record of loess and soil (binary data) and REDFIT method spectra of the frequency dependence (FD) parameter. The gray thick line indicates the first-order autoregressive (AR1) red noise model fit. The peaks at 1500, 1000 and ~600 year periods are significantly above the noise level. Vertical lines indicate the millennium scale periodicities (in kyr).

and Icelandic loess grain size variation (Jackson et al., 2005) (Fig. 6). Such correspondence illustrates the global connections between the oceanic climate of the North Atlantic, the continental climate in central Eurasia, and the parameters that represent solar activity. Since Denton and Karlén (1973) suggested that advance and retreat of glaciers occur in 1500-year cycles, many studies have reported climatic oscillations of 2500, 1500, and 1000 years (Bond et al., 1997; Bianchi and McCave, 1999; Viau et al., 2006; Debret et al., 2009). During the Holocene, natural climate cycles of 1500 years appear to be persistent, although the origin of this pacing remains unexplained (Bond et al., 2001; Rahmstorf, 2003; Mayewski et al., 2004). Solar variability is often considered to be responsible for such cycles, but the evidence for solar forcing is difficult to evaluate in the presence of many other components.

Debret et al. (2007) demonstrated the advantage of the wavelet analysis (WA) as compared to the classical Fourier spectral analysis (usually Blackman–Tukey or maximum entropy technique) while detecting a 1500-year periodicity that evolves through time in the oceanic records. These authors (2007) argued that this type of spectral analysis of existing oceanic data sets has enabled them to distinguish 1000- and 2500-year oscillations of solar forcing and has revealed that 1500-year climate cycles are linked to oceanic circulation in the latter half of Holocene.

First, we used the PAST software (Hammer et al., 2001) to apply the Walsh transform to our lithological binary record considering loess as zero and soil as one on the equally spaced time scale. Fig. 7 demonstrates that the lithological record comprises a dominant peak of 1000 year periodicity. We also compared our results with the REDFIT spectral analysis module (Hammer et al., 2001) described in Schulz and Mudelsee (2002) for our FD data (Fig. 7). The time series is fitted to a red noise model in this method. We also compared REDFIT with the Blackman–Tukey method spectra (not shown, using software of Paillard et al., 1996). The cycles of 1000 and ~500 years are the same for both techniques; the period of 1500 year is veiled in the Blackman–Tukey spectrogram.

Secondly, we performed WA on the FD record and Drift Ice Indices Stack (Bond et al., 2001) in order to evaluate the subtle changes through time and to compare our results with the global records (Fig. 8) (see Debret et al. (2007, 2009) for discussion and illustration of the WA analysis of the other oceanic records). In order to perform the analysis we modified the Matlab code from Torrence and Compo (1998) and used the Morlet wavelet described in Debret et al. (2007). WA performed on FD time series highlights major cyclicities (at 95% of confidence): the most prominent 1000 year cycle throughout whole Holocene, and ~500 and ~1500 year between 2 and 5 ka (Fig. 8). WA performed on the Drift Ice Indices Stack reveals three

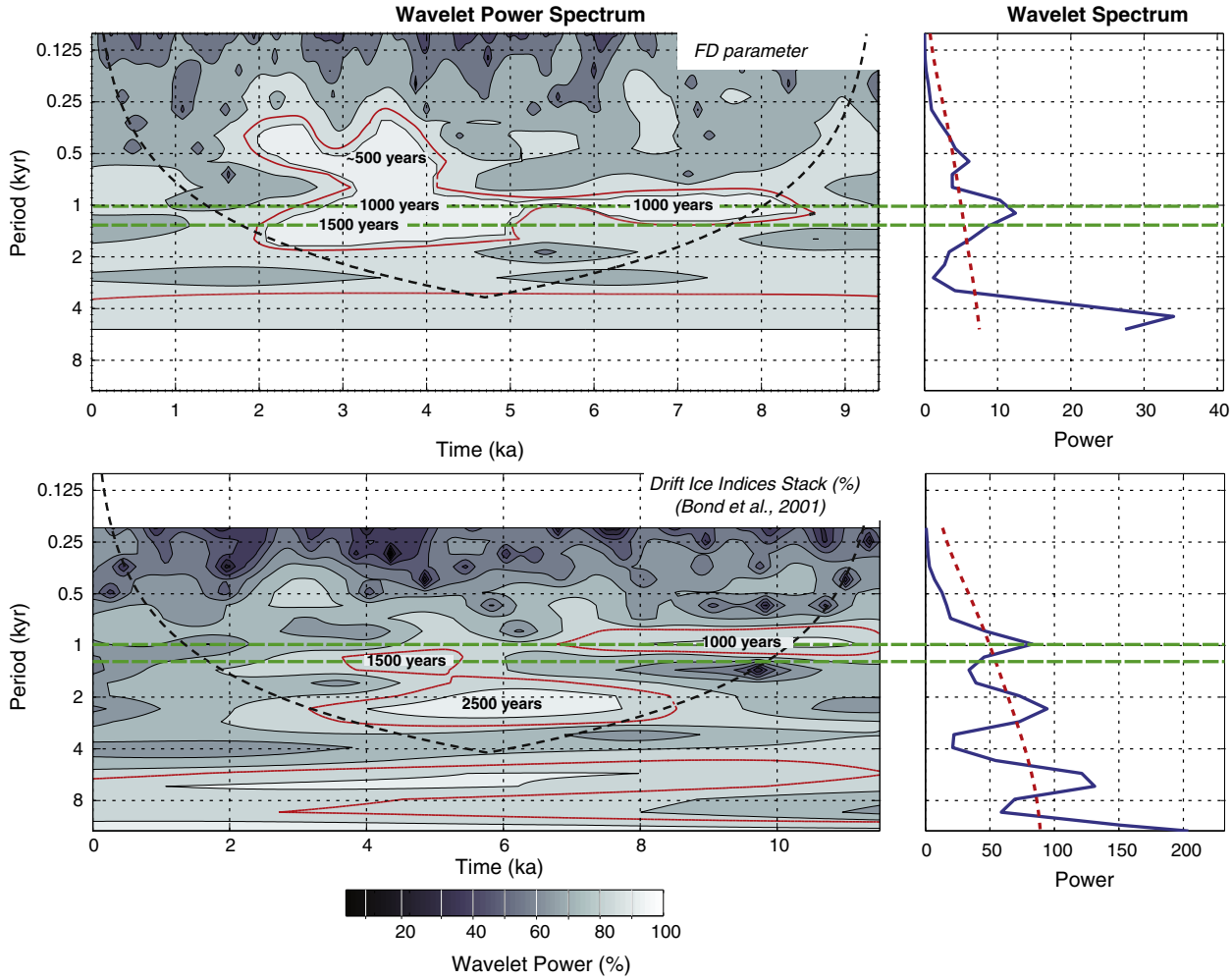

Fig. 8. Wavelet transform analysis of the 9500 year long FD-factor record for the Burdukovo Holocene section (this study) and Drift Ice Indices Stack (Bond et al., 2001). Occurrence of the periods (labeled) with respect to the time is given by the lighter gray color. Black dashed line corresponds to cone of influence. The confidence levels (more than 95%) are indicated with the red line. Fourier power spectrum of is given to the right. The red dashed line is the mean red noise spectrum (a lag of 0.72 for FD and 0.4 for Drift Ice Indices Stack). The upper dashed line is the 95% confidence spectrum.

major cyclicities: 1000, 1500 and 2500 years (Fig. 8). This wavelet power spectrum is identical to the spectrum of Debret et al. (2007), their Fig. 3). The 1000 year cycle is absent from present to 5 ka; spectral power increases at a period of ~1500 years.

Our result for the WA spectrum of FD is in line with the records of ^{10}Be and especially ^{14}C where the 1000 years period is strong and ~1500 years is very weak (below the confidence level) (see Fig. 3 in Debret et al., 2009). The concentration of these isotopes depends on the amount of solar radiation and can therefore be expected to show spectra similar to sun spot number and solar modulation spectra.

We performed WA analyses on sun spot number and solar insolation in order to compare their spectra with the FD parameter spectrum in Fig. 8. The spectra show that the 2500-year cycle is the most prominent in the spectrum of the sun spot number (Fig. 9). The period of 1000 years is significant in the interval between 7 and 11 ka, which is similar to the WA power spectrum for the Drift Ice Indices Stack in Fig. 8. The 500-year cycle is significant at 2–3.5 ka and 8.5–10 kyr. The first interval is observed in the FD spectrum, the second cannot be resolved in our study as the FD record goes only until 9.5 ka. The solar insolation WA spectrum is characterized by the dominant 1000-year cycle which is most significant in both the FD and solar insolation between 3 and 9 ka and visible from the present day to 1–1.5 ka.

Our section is remote from an ocean and therefore oceanic circulation is expected to play only a minor role in this deep continental area, whereas solar radiation could be amplified by the harsh continental climate conditions. Fig. 10 illustrates that the FD parameter spectrum is coherent to both sun spot number and solar modulation spectra at the statistically significant peaks of 1000 and 500 years. The coherency is calculated with the Blackman–Tukey method (Blackman and Tukey, 1958) with a Bartlett window. The procedure follows Paillard et al. (1996) and uses the authors' software.

Hence, our results support the arguments of Debret et al. (2007) that the 1000-year cycle is directly forced by solar activity whereas the ~1500-year cycle, dominant during the Late Holocene, most likely corresponds to oceanic internal forcing. Our data do not indicate any presence of the 2500-year cycle shown in the oceanic record and sunspot number spectra. The solar insolation data of Beer et al. (2006) also do not contain this cycle although the sun spot number does (Fig. 9). From the FD data set it appears that the 1500-year cycle may have a global distribution.

It is not clear that a change of 1.5 W/m^2 in Holocene solar radiation (Usoskin et al., 2007) can explain a direct influence of solar variability on climatic change. Beer et al. (2006) briefly reviewed possible feedback mechanisms that could amplify the solar heating effect. We demonstrate here that continental climate change with periodicities of ~500 and 1000 years is more easily linked to solar variability in the Holocene whereby the oceanic cycle of ~1500 years is still in effect in the Late Holocene.

6. Conclusions

(1) We constructed a complete Holocene climate record in the center of the Eurasian continent that corresponds to global climate records from the North Atlantic, to sun spot number, and to the amount of solar insolation.

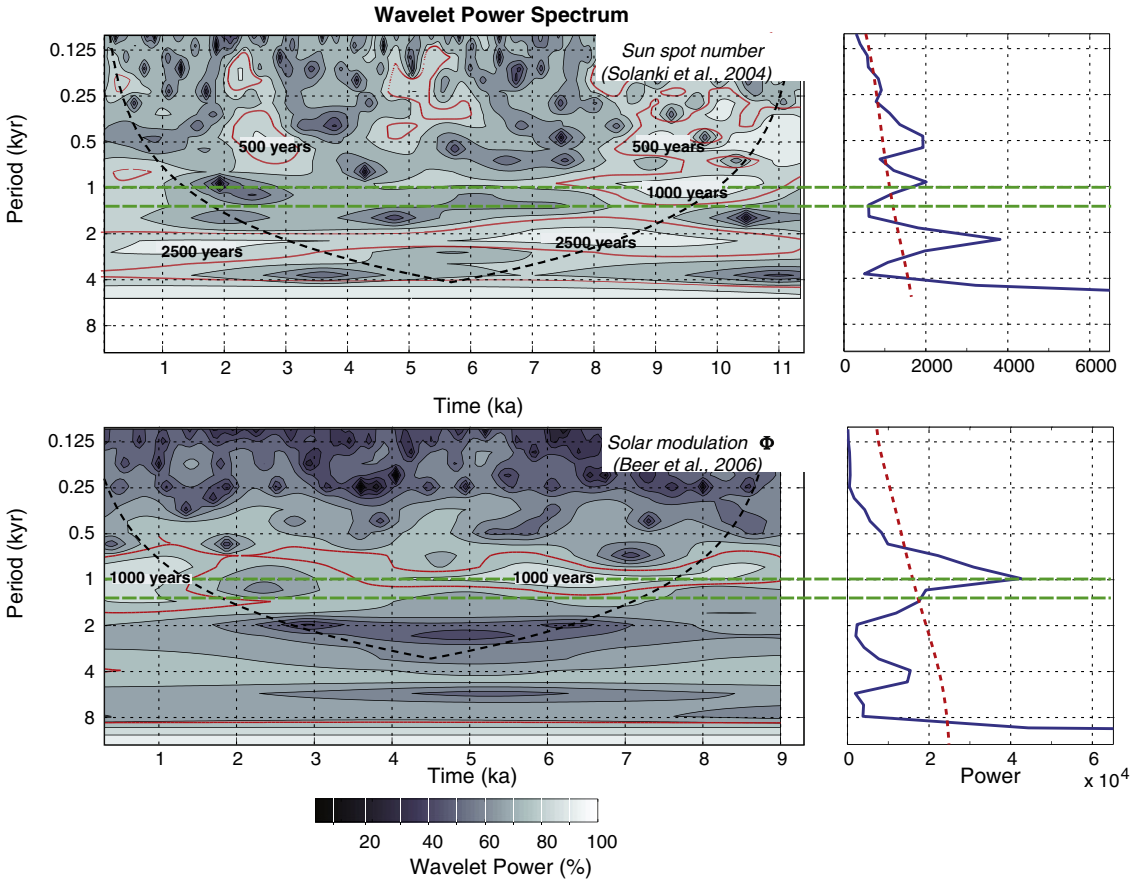

Fig. 9. Wavelet transform analysis of the sun spot number (data from Solanki et al., 2004), and solar modulation parameter Φ (data from Beer et al., 2006). Occurrence of the periods (labeled) with respect to the time is given by the lighter gray color. Black dashed line corresponds to cone of influence. The confidence levels (more than 95%) are indicated with the red line. Fourier power spectrum of is given to the right. The red dashed line is the mean red noise spectrum (a lag of 0.1 for sun spot number and 0.4 for solar modulation). The upper dashed line is the 95% confidence spectrum.

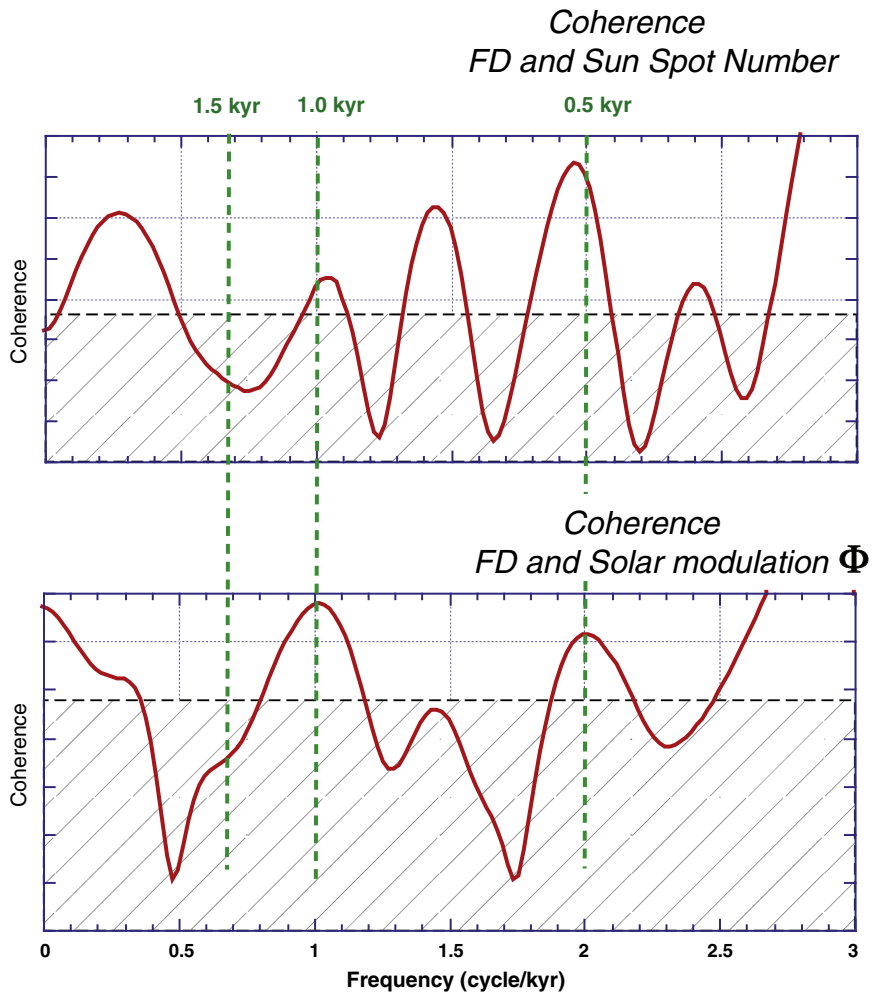

Fig. 10. The coherence between the 9500 year long FD-factor record for the Burdukovo Holocene section (this study) and sun spot number (data from Solanki et al., 2004) and between FD and solar modulation parameter Φ (data from Beer et al., 2006). Horizontal dashed line corresponds to the 95% confidence level. The analysis was performed with the Blackman–Tukey technique using a Bartlett window using a 50 year step, signal band-width of 0.5, and 420 lags. Vertical lines indicate the millennium scale periodicities (in kyr).

(2) Spectral analyses of this record reveal persistent periodicities of 1000 and 500 years that may correspond to solar activity variations during the Holocene epoch. Such periods correspond to solar variation induced climate changes and are recorded in magnetic properties of soil layers deposited during cyclic changes in the environment.
(3) A 1500 year cycle corresponding to the North Atlantic oceanic circulation may have widespread global distribution in the Late Holocene.
(4) Three time periods — 8400–9300, 3600–5100 years BP, and the last ~250 years BP — correspond to both the highest sun spot number and the most developed soil horizons in the studied section. We suggest that the first of the three time intervals relates to the warmer period registered in the Greenland temperature and Siberian pollen records, the second time period correlates to the middle–late Holocene warmer and wetter period registered in the Lake Baikal oxygen isotope and pollen record and the most recent time period matches the post Little Ice Age warming.

Acknowledgments

We thank A. Weber, A. Shchetnikov and L.P. Koukhar for their help in the field and during laboratory measurements. The study was partially funded by the Natural Sciences and Engineering Research Council of Canada (NSERC) and Infrastructure Operating Fund of Canada Foundation for Innovation (IOF-CFI) (grants of V.K.). The paper benefitted considerably from the comments and suggestions of S. Spassov and an anonymous reviewer.

Data availability

With this contribution we release the data to public domain, the data is downloadable at http://www.pangaea.de/

Appendix A. Supplementary data

Supplementary data to this article can be found online at http://dx.doi.org/10.1016/j.gloplacha.2013.02.011.

References

Bábek, O., Chlachula, J., Grygar, T.M., 2011. Non-magnetic indicators of pedogenesis related to loess magnetic enhancement and depletion: examples from the Czech Republic and southern Siberia. Quaternary Science Reviews 30, 967–979.
Bard, E., Delaygue, G., 2008. Comment on "Are there connections between the Earth's magnetic field and climate?" by V. Courtillot, Y. Gallet, J.-L. Le Mouël, F. Fluteau, A. Genevey EPSL 253, 328, 2007. Earth and Planetary Science Letters 265, 302–307.
Beer, J., Vonmoos, M., Muscheler, R., 2006. Solar variability over the past several millennia. Space Science Reviews 125, 67–79.

Bianchi, G.G., McCave, I.N., 1999. Holocene periodicity in North Atlantic climate and deep-ocean flow south of Iceland. Nature 397, 515–517.
Blackman, R.B., Tukey, J.W., 1958. The Measurement of Power Spectra From the Point of View of Communication Engineering.Diver Publications.
Bloemendal, J., Liu, X.M., 2005. Rock magnetism and geochemistry of two Plio-Pleistocene Chinese loess–palaeosol sequences — implications for quantitative palaeoprecipitation reconstruction. Palaeogeography, Palaeoclimatology, Palaeoecology 226, 149–166.
Bond, G., Showers, W., Cheseby, M., Lotti, R., Almasi, P., deMenocal, P., Priore, P., Cullen, H., Hajdas, I., Bonani, G., 1997. A pervasive millennial-scale cycle in North Atlantic Holocene and glacial climates. Science 278, 1257–1266.
Bond, G., Kromer, B., Beer, J., Muscheler, R., Evans, M.N., Showers, W., Hoffmann, S., Lotti-Bond, R., Hajdas, I., Bonani, G., 2001. Persistent solar influence on north Atlantic climate during the Holocene. Science 294, 2130–2136.
Carlson, A.E., Clark, P.U., Raisbeck, G.M., Brook, E.J., 2007. Rapid Holocene deglaciation of the Labrador sector of the Laurentide ice sheet. Journal of Climate 20, 5126–5133.
Coombes, P., Barber, K., 2005. Environmental determinism in Holocene research: causality or coincidence? Area 37-3, 303–311.
Courtillot, V., Gallet, Y., Le Mouel, J.L., Fluteau, F., Genevey, A., 2007. Are there connections between the Earth's magnetic field and climate? Earth and Planetary Science Letters 253 (3–4), 328–339.
Courtillot, V., Gallet, Y., Le Mouel, J.L., Fluteau, F., Genevey, A., 2008. Response to comment on — "Are there connections between Earth's magnetic field and climate?". Earth and Planetary Science Letters 265 (1–2), 308–311.
Day, J.W., Gunn, J.D., Folan, W.J., Yáñez-Arancibia, A., Horton, B.P., 2007. Emergence of complex societies after sea level stabilized. EOS. Transactions of the American Geophysical Union 88, 169. http://dx.doi.org/10.1029/2007EO150001.
Debret, M., Bout-Roumazeilles, V., Grousset, F., Desmet, M., McManus, J.F., Massei, N., Sebag, D., Petit, J.-R., Copard, Y., Trentesaux, A., 2007. The origin of the 1500-year climate cycles in Holocene North-Atlantic records. Climate of the Past 3, 569–575.
Debret, M., Sebag, D., Crosta, X., Massei, N., Petit, J.-R., Chapron, E., Bout-Roumazeilles, V., 2009. Evidence from wavelet analysis for a mid-Holocene transition in global climate forcing. Quaternary Science Reviews 28, 2675–2688.
DeMenocal, P.B., 2001. Cultural responses to climate change during the Late Holocene. Science 292 (5517), 667–673.
Denton, G.H., Karlén, W., 1973. Holocene climatic variations — their pattern and possible cause. Quaternary Research 3, 155–205.
Evans, M.E., Heller, F., 2001. Magnetism of loess/palaeosol sequences: recent developments. Earth-Science Reviews 54, 129–144.
Friis-Chrisensen, E., Svensmark, H., 1997. What do we really know about the sun–climate connection? Advances in Space Research 20, 913–921.
Gallet, Y., Genevey, A., 2007. The Mayans: climate determinism or geomagnetic determinism? EOS 88 (11).
Gallet, Y., Genevey, A., Courtillot, V., 2003. On the possible occurrence of 'archaeomagnetic jerks' in the geomagnetic field over the past three millennia. Earth and Planetary Science Letters 214 (1–2), 237–242.
Gallet, Y., Genevey, A., Le Goff, M., Fluteau, F., Ali Eshraghi, S., 2006. Possible impact of the Earth's magnetic field on the history of ancient civilizations. Earth and Planetary Science Letters 246 (1–2), 17–26.
Hammer, Ø., Harper, D.A.T., Ryan, P.D., 2001. PAST: paleontological statistics software package for education and data analysis. Palaeontologia Electronica 4 (1) (9 pp.,).
International Society of Soil Science, 1998. World reference base for soil resources: world soil resources report, no. 84. International Soil Reference and Information Center.United Nations Food and Agriculture Organisation, Rome, Italy.
Jackson, M.G., Oskarson, N., Trønnes, R.G., McManus, J.F., Oppo, D., Grönveld, K., Hart, S.R., Sachs, J.P., 2005. Holocene loess deposition in Iceland: evidence for millennial-scale atmosphere–ocean coupling in the North-Atlantic. Geology 33, 509–512.
Kravchinsky, V.A., Evans, M.E., Peck, J.A., Sakai, H., Krainov, M.A., King, J.W., Kuzmin, M.I., 2007. A 640 kyr geomagnetic and paleoclimatic record from Lake Baikal sediments. Geophysical Journal International 101, 101–116.
Kravchinsky, V.A., Zykina, V.S., Zykin, V.S., 2008. Magnetic indicator of global paleoclimate cycles in Siberian loess–paleosol sequence. Earth and Planetary Science Letters 265, 498–514.
Mackay, A.W., Swann, G.E.A., Brewer, T., Leng, M.J., Morley, D.W., Piotrowska, N., Rioual, P., White, D., 2011. A reassessment of late glacial-Holocene diatom oxygen isotope records from Lake Baikal using a mass balance approach. Journal of Quaternary Science 26 (6), 627–634.
Magny, M., Bossuet, G., Ruffaldi, P., Leroux, A., Mouthon, J., 2011. Orbital imprint on Holocene palaeohydrological variations in west-central Europe as reflected by lake-level changes at Cerin (Jura Mountains, eastern France). Journal of Quaternary Science 26, 171–177.
Mayewski, P.A., Rohling, E.E., Stager, J.C., Karlen, W., Maasch, K.A., Meeker, L.D., Meyerson, E.A., Gasse, F., van Kreveld, S., Holmgren, K., Lee-Thorp, J., Rosqvist, G., Rack, F., Staubwasser, M., Schneider, R.R., Steig, E.J., 2004. Holocene climate variability. Quaternary Research 62, 243–255.
Paillard, D., Labeyrie, L., Yiou, P., 1996. Macintosh program performs time series analysis. Transactions of the American Geophysical Union (EOS) 77, 379.
Rahmstorf, S., 2003. Timing of abrupt climate change: a precise clock. Geophysical Research Letters 30, 1510. http://dx.doi.org/10.1029/1003GL017115.
Rahmstorf, S., 2006. Thermohaline ocean circulation. In: Elias, S.A. (Ed.), Encyclopedia of Quaternary Sciences. Elsevier, Amsterdam.
Ramsey, C.B., 2001. Development of the radiocarbon program OxCal. Radiocarbon 43 (2A), 355–363.
Reimer, P.J., Baillie, M.G.L., Bard, E., Bayliss, A., Beck, J.W., Bertrand, C., Blackwell, P.G., Buck, C.E., Burr, G., Cutler, K.B., Damon, P.E., Edwards, R.L., Fairbanks, R.G., Friedrich, M., Guilderson, T.P., Hughen, K.A., Kromer, B., McCormac, F.G., Manning, S., Ramsey, C.B., Reimer, R.W., Remmele, S., Southon, J.R., Stuiver, M., Talamo, S., Taylor, F.W., van der Plicht, J., Weyhenmeyer, C.E., 2004. IntCal04 terrestrial radiocarbon age calibration, 0–26 cal kyr BP. Radiocarbon 46, 1029–1058.
Schulz, M., Mudelsee, M., 2002. REDFIT: estimating red-noise spectra directly from unevenly spaced paleoclimatic time series. Computers & Geosciences 28, 421–426.
Schulz, M., Paul, A., 2002. Holocene climate variability on centennial-to-millennial time scales: 1. Climate records from the North-Atlantic realm. In: Wefer, G., Berger, W., Behre, K.E., Jansen, E. (Eds.), Climate Development and History of the North Atlantic Realm. Springer-Verlag, Berlin Heidelberg, pp. 41–54.
Soil Classification Working Group, 1998. The Canadian system of soil classification. Agriculture and Agri-Food Canada Publication 1646.NRC Research Press, Ottawa, Ontario, Canada.
Solanki, S.K., Usoskin, I.G., Kromer, B., Schüssler, M., Beer, J., 2004. An unusually active Sun during recent decades compared to the previous 11,000 years. Nature 431 (7012), 1084–1087.
Staubwasser, M., Weiss, H., 2006. Holocene climate and cultural evolution in late prehistoric–early historic West Asia. Quaternary Research 66, 372–387.
Tarasov, P., Bezrukova, E., Karabanov, E., Nakagawa, T., Wagner, M., Kulagina, N., Letunova, P., Abzaeva, A., Granoszewski, W., Riedel, F., 2007. Vegetation and climate dynamics during the Holocene and Eemian interglacials derived from Lake Baikal pollen records. Palaeogeography, Palaeoclimatology, Palaeoecology 252, 440–457.
Torrence, C., Compo, G.P., 1998. A practical guide to wavelet analysis. Bulletin of the American Meteorological Society 79, 61–78.
Usoskin, I.G., Solanki, S.K., Kovaltsov, G.A., 2007. Grand minima and maxima of solar activity: new observational constraints. Astronomy and Astrophysics 471, 301–309.
Viau, A.E., Gajewski, K., Sawada, M.C., Fines, P., 2006. Millennial-scale temperature variations in North America during the Holocene. Journal of Geophysical Research 111, D09102. http://dx.doi.org/10.1029/2005JD006031.
Vinther, B.M., Buchardt, S.L., Clausen, H.B., Dahl-Jensen, D., Johnsen, S.J., Fisher, D.A., Koerner, R.M., Raynaud, D., Lipenkov, V., Andersen, K.K., Blunier, T., Rasmussen, S.O., Steffensen, J.P., Svensson, A.M., 2009. Holocene thinning of the Greenland ice sheet. Nature 461, 385–388.
Vonmoos, M., Beer, J., Muscheler, R., 2006. Large variations in Holocene solar activity: constraints from ^{10}Be in the Greenland Ice Core Project ice core. Journal of Geophysical Research 111 (A10105). http://dx.doi.org/10.1029/2005JA011500.
White, D., 2006. Holocene climate and culture change in the Lake Baikal Region, Siberia. Ph.D. thesis, University of Alberta, Canada.
White, D., Preece, R.C., Shchetnikov, A.A., Dlussky, K.G., 2013. Late Glacial and Holocene environmental change reconstructed from floodplain and aeolian sediments near Burdukovo, Lower Selenga River Valley (Lake Baikal region), Siberia. Quaternary International 290–291, 68–81.

Appendix A. Supplementary Materials

Discovery of Holocene millennial climate cycles in the Asian continental interior: Has the sun been governing the continental climate?

Vadim A. Kravchinsky [1,2,*], Cor G. Langereis [2], Shawn D. Walker [1],

Konstantin G. Dlusskiy [3,4], Dustin White [3,5]

[1] *Physics Department, University of Alberta, Edmonton, Alberta, Canada T6G 2G7*

[2] *Department of Earth Sciences, Utrecht University, Budapestlaan 17, 3584 CD Utrecht, the Netherlands*

[3] *Department of Anthropology, University of Alberta, Edmonton, Alberta, Canada T6G 2H4*

[4] *Now at Solstice Canada Corp., Edmonton, Alberta, Canada T5M 0H1*

[5] *Now at Archaeology, University of Southampton, Southampton SO17 1BJ, UK*

[*] *Corresponding author: Tel.: +1-(780)-492-5591; Fax: +1-(780)-492-0714; E-mail address: vadim@ualberta.ca*

Global and Planetary Change

2013

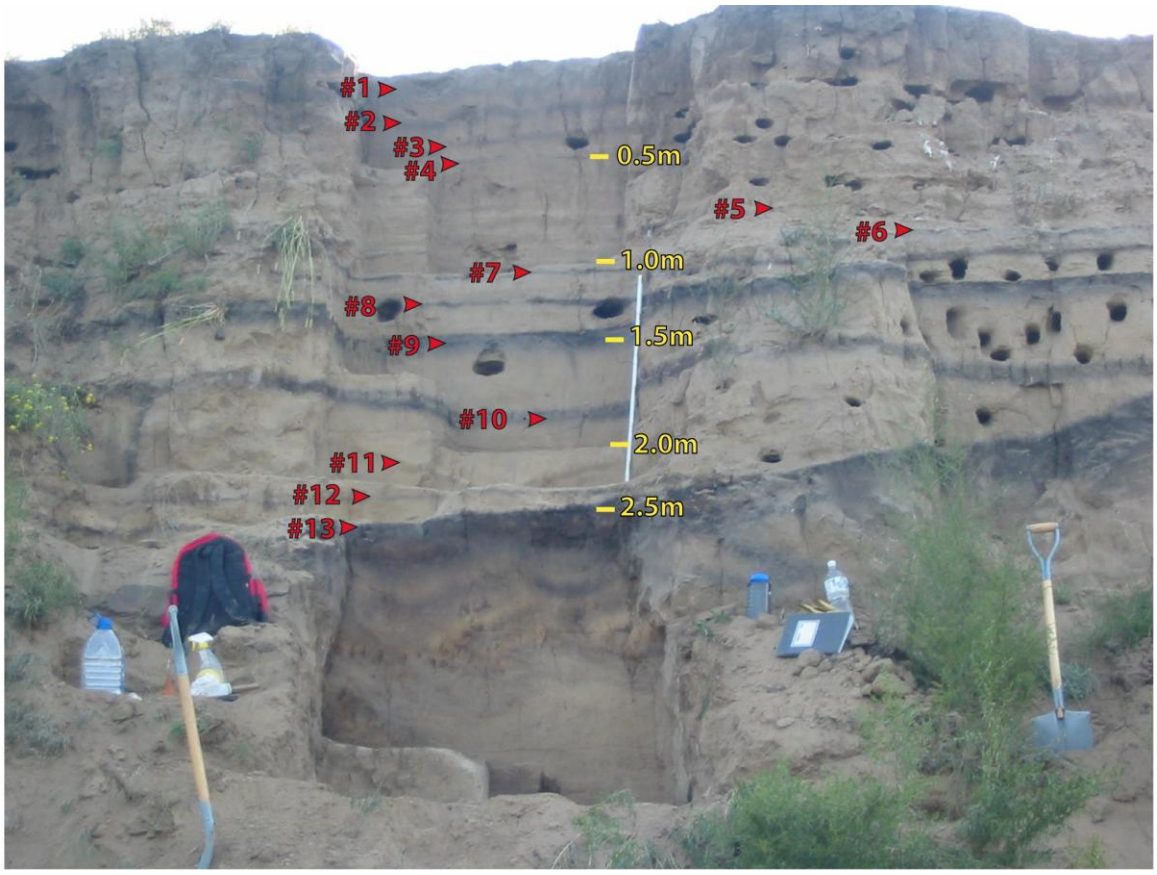

Figure SM-1. Loess / buried soil sequence of Trench 1. Numbers near arrows indicate soil horizons which correspond to Figure 3 and 4 of the manuscript.

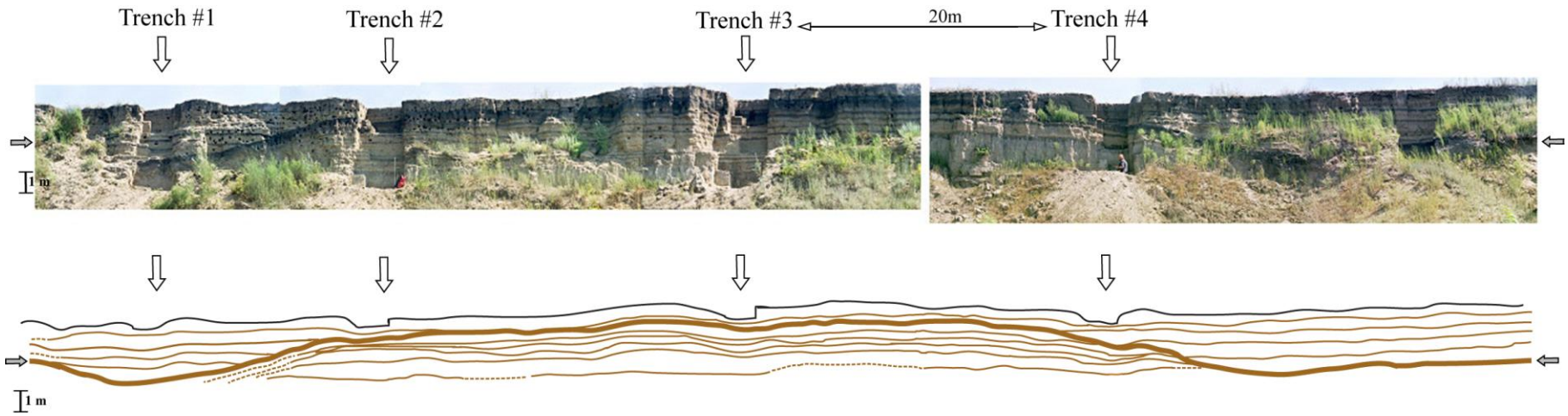

Figure SM-2. Top: the Burdukovo study site trench photo. Trench 1 is at the base of the paleo-depression, Trenches 2 and 4 are in a transitional zone, Trench 3 is on a plateau. The grey horizontal arrows on either side of the figure are indicating the top of soil #13, the thickest buried soil. Bottom: a highlight of a few most pronounced soils and their continuity.

Methods

Petromagnetic parameters

We used 8 cm^3 plastic non-magnetic boxes to host the sediments for petromagnetic measurements. Magnetic susceptibility was measured with a Bartington Instruments single-sample dual frequency sensor (0.43 and 4.3 kHz) in order to calculate frequency dependence (FD parameter in %). Anhysteric remanent magnetization (ARM) was induced in the samples with a 2-G cryogenic magnetometer demagnetizer operating at a peak AF field of 0.1 T and a steady field of 0.1 mT and measured on the cryogenic magnetometer. The ARM was normalized to the steady field and expressed as χ_{ARM}. Saturation isothermal remanent magnetization (SIRM) was induced in the samples by a 2-G IRM stand-along electromagnet using a field of 0.6 T. An induced back IRM (bIRM) was applied to the samples by subjecting them to a reversed field of 0.3 T generated by the electromagnet. The magnetizations were measured on the cryogenic magnetometer.

Petromagnetic parameters χ_{lf}, χ_{ARM} and SIRM indicate primarily variations in magnetic mineral concentration (Thompson and Oldfield, 1986; Robinson, 1986; Yu and Oldfield, 1989; King and Channell, 1991; Evans and Heller, 2003). The parameter values rise when the concentration of magnetic material in the sediment increases. Both χ_{ARM} and SIRM are magnetic grain-size dependent and increase in value with an increase in concentration of single domain magnetic grain sizes. χ_{lf} is also grain-size dependent, with higher values at both larger magnetic grain sizes (multidomain) and very fine magnetic grain sizes (superparamagnetic).

The studied samples do not show a notable dependence of magnetic susceptibility on sedimentary grain size. MS values are determined by the concentration of low coercivity minerals (i.e., magnetite and maghemite). SIRM is also dependent on magnetic mineralogy, with minerals having a high magnetization (e.g., magnetite) contributing to a larger SIRM value. Unlike χ_{ARM} and SIRM which measure magnetic remanences only, χ is measured in a weak magnetic field so that non-remanent (diamagnetic and paramagnetic) sediment components contribute to it. When remanence bearing minerals occur in low concentration, the diamagnetic and paramagnetic components can significantly influence χ.

The interparametric ratios χ_{ARM}/χ and χ_{ARM}/SIRM indicate variations primarily in magnetic grain size. These ratios vary inversely with magnetic grain size (Thompson and Oldfield, 1986; King et al., 1982; Maher, 1988; Evans and Heller, 2003). Both ratios primarily reflect the presence of finer magnetic grain sizes (single domain) and can be used to assess the relative change in concentration of finer magnetic grain sizes (Blomendal et al., 1993).

The interparametric ratio S reflects variations in the coercivity spectrum of the magnetic mineral assemblage and therefore in the mineralogy (Robinson, 1986; Thompson and Oldfield, 1986; King and Channel, 1991). S-ratio values vary from zero to one. The value of one corresponds to pure magnetite/maghemite and decreases with growing proportion of antiferromagnetic grains (hematite/goethite).

In addition to the FD and the grain size analyses a high temperature magnetic susceptibility was performed on several samples using a Bartington MS2W system. The temperature of the samples was increased from room temperature to 700°C and the magnetic susceptibility was measured every 2°C. Once the samples had finished heating to 700°C, they were allowed to cool to room temperature and the magnetic susceptibility was taken at 2°C increments. At 380°C all samples show a change in the rate of increasing magnetic susceptibility (MS) (Figure SM-3). The MS of all samples increase until the temperature reaches approximately 555°C, and all show sharp decreases from 570°C to 580°C. The samples also show an increase in magnetic susceptibility at approximately 270°C. Others have previously interpreted this anomaly as a thermally triggered change of metastable maghemite (γ-Fe_2O_3) to hematite (α-Fe_2O_3) (Zhu et al, 2003). The anomaly observed in our samples is much smaller than is observed in other studies and indicates that any maghemite present likely occurs in only trace amounts. After reaching minimum magnetic susceptibilities at approximately 590°C, all samples started to steadily increase in magnetic susceptibility to our end temperature of 700°C. The increase in magnetic susceptibility after 590°C is likely due to the presence of hematite, either initial hematite or hematite produced by the reduction of maghemite at increased temperature.

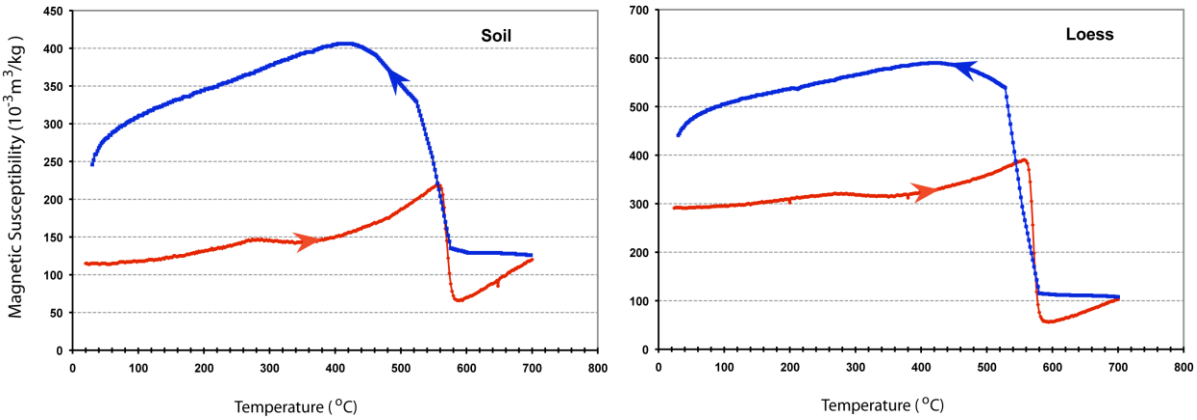

Figure SM-3. Magnetic susceptibility measurements of three samples from Trench 1 as temperature was increased from room temperature to 700°C (red line) and cooled back to room temperature (blue line).

Sedimentary grain size analysis

Grain size analysis was performed in order to determine relative wind strengths during loess deposition. Testing of the grain size was performed using sieves and a Sedigraph 5100. Samples were first air dried and then crushed using a mortar and pestle and dry sieved through a 1 mm sieve. After dry sieving, a subsample between 5 and 10 g was then oven dried over night to remove all moisture from the sample. The sample was then weighed and a 5% sodium metaphosphate solution was added, to break down any post-depositional cementation, and allowed to sit for 8 hours. The sample was then wet sieved through 100 µm, 250 µm, and 500 µm sieves. The material in the 100 µm to 250 µm, 250 µm to 500 µm, and 500 µm to 1mm ranges were then completely dried and weighed. The proportion of material that was less than 100 µm was left in solution and allowed to evaporate down to approximately 40 ml to 50 ml of solution and sediment. The sediment solution mixture was then agitated and placed in the mixing chamber of the Sedigraph. The mixture was then mechanically loaded into the analysis cell and analysed with a beam of x-rays. The x-rays are shot through the clear window of the analysis cell and are diffracted by the particles as they settle. The diffraction of the x-rays are measured and used to determine the grain size diameter. For this analysis the grain size analysis was separated into diameter ranges of; less than 0.98 µm, 0.98 to 2 µm, 2 to 5 µm, 5 to 10 µm, 10 to 20 µm, 20 to 50 µm, and from 50 to 100 µm. These grain sizes ranges were used as they are the standard grain sizes used in pedogenic studies (Pansu and Gautheyrou, 2006). We also measured the median grain size, which appeared to be a better parameter to demonstrate a dependency on relative wind strength for our study.

Additional references

Arnold, J.R., Libby, W.F., 1949. Age Determinations by Radiocarbon Content: Checks with Samples of Known Age, Science 110 (2869), 678–680.

Blomendal, J., King, J.W. Hunt A., DeMenocal P.B. Hayashida A., 1993. Origin of the sedimentary magnetic record at Ocean Drilling Program sites on the Owen Ridge, Western Arabian Sea, J. Geophys. Res. 98, 4199-4219.

Demory, F., Oberhansli, H., Nowaczyk, N.R., Gottschalk, M., Wirth, R., Naumann, R., 2005. Detrital input and early diagenesis in sediments from Lake Baikal revealed by rock magnetism. Glob. Planet. Change 46, 145–166.

Evans, M.E., Heller, F., 2003. EnvironmentalMagnetism: Principles and Applications of Enviromagnetics, Elsevier Science, Academic Press.

Jackson, M.G., Oskarson, N, Trønnes, R. G., McManus, J. F., Oppo, D., Grönveld, K., Hart, S. R., and Sachs, J. P., 2005. Holocene loess deposition in Iceland: Evidence for millennialscale atmosphere-ocean coupling in the North-Atlantic. Geology 33, 509–512.

King, J.W., Banerjee, S.K., Marvin, J., Ozdemir O., 1982. A comparison of different magnetic methods for determining the relative grain size of magnetite in natural materials: some results from lake sediments, Earth Planet. Sci. Lett. 59, 404-419.

King, J.W., Channell, J.E.T., 1991. Sedimentary magnetism, environmental magnetism, and magnetostratigraphy, Rev. Geophys., 358–370, 1991 (Suppl.).

Maher, B.A., 1988. Magnetic properties of some synthetic submicron magnetite, Geophys. J. 94, 83–96.

Pansu, M., Gautheyrou, J., 2006. Handbook of Soil Analysis: Mineralogical, Organic and Inorganic Methods. Berlin Heidelberg: Springer-Verlag.

Robinson, S.G., 1986. The late Pleistocene paleoclimatic record of North Atlantic deep-sea sediments revealed by mineral-magnetic measurements, Phys. Earth Planet. Inter. 42, 22–47.

Thompson, R., Oldfield, F., 1986. Environmental Magnetism, Allen and Unwin, London.

Yu, L., Oldfield, F., 1989. A multivariate mixing model for identifying sediment source from magnetic measurements, Quaternary Research 32, 168–181.